ResearchGate

See discussions, stats, and author profiles for this publication at: https://www.researchgate.net/publication/318857003

Collective Behavior of Chiral Active Matter: Pattern Formation and Enhanced Flocking

Article *in* Physical Review Letters · August 2017

DOI: 10.1103/PhysRevLett.119.058002

CITATIONS
13

READS
124

2 authors, including:

Demian Levis
University of Barcelona
19 PUBLICATIONS **237** CITATIONS

SEE PROFILE

All content following this page was uploaded by Demian Levis on 06 September 2017.

The user has requested enhancement of the downloaded file.

Collective Behaviour of Chiral Active Matter: Pattern Formation and Enhanced Flocking

Benno Liebchen[1,*] and Demian Levis[2,3,†]

[1] *SUPA, School of Physics and Astronomy, University of Edinburgh, Edinburgh EH9 3FD, United Kingdom*
[2] *Departament de Física de la Matèria Condensada, Universitat de Barcelona, Martí i Franquès 1, E08028 Barcelona, Spain*
[3] *Universitat de Barcelona Institute of Complex Systems (UBICS), Universitat de Barcelona, E08028 Barcelona, Spain*

(Dated: July 13, 2017)

We generalize the Vicsek model to describe the collective behaviour of polar circle swimmers with local alignment interactions. While the phase transition leading to collective motion in 2D (flocking) occurs at the same interaction to noise ratio as for linear swimmers, as we show, circular motion enhances the polarization in the ordered phase (enhanced flocking) and induces secondary instabilities leading to structure formation. Slow rotations promote macroscopic droplets with late time sizes proportional to the system size (indicating phase separation) whereas fast rotations generate patterns consisting of phase synchronized microflocks with a controllable characteristic size proportional to the average single-particle swimming radius. Our results defy the viewpoint that monofrequent rotations form a vapid extension of the Vicsek model and establish a generic route to pattern formation in chiral active matter with possible applications to understand and design rotating microflocks.

Among the most remarkable features of active matter systems is their ability to spontaneously form self-sustained nonequilibrium structures, without requiring external driving. These active structures range from motility-induced phase separation of self-propelled particles into a dense and a dilute phase [1, 2] and clusters of self-limited size [3–7] in isotropic active matter, to long range ordered flocks and travelling bands in 2D polar active matter [8–12]. Despite their phenomenological diversity most of these (and other) activity-induced structures can be observed in a small class of archetypical minimal models allowing to explore their universality. For linear self-propelled particles which change their swimming direction only by diffusion (and alignment interactions), the Active Brownian Particle model and the Vicsek model have become standard models representing isotropic and polar active matter.

Besides such linear swimmers, there is now a strong interest in a new class of self-propelled particles which change their direction of motion autonomously. This class of chiral active matter includes a variety of biological circle swimmers, such as *E.coli* which swim circularly when close to walls and interfaces [16–19], as well as sperm cells [20, 21], and magnetotactic bacteria in rotating external fields [22, 23]. Following the general principle that any deviation between the self-propulsion direction of the particle and its symmetry axis couples its translational and rotational degrees of freedom, it has also been possible to design synthetic circle swimmers; examples being L-shaped self-phoretic swimmers [24, 25] and actuated colloids allowing to design radius and frequency of circular trajectories on demand. While these synthetic examples have supported the recent boost of interest in chiral active matter, as the recent reviews [26, 27] reflect, surprisingly little is known about their collective behaviour (exceptions exploring collective behaviour are [13, 28, 29]).

Therefore, following the spirit of formulating minimal models for the collective behavior of linear active matter, we introduce here the *Chiral Active Particle* model (CAP) to describe the collective behavior of polar circle swimmers. The CAP describes overdamped self-propelled particles changing their direction autonomously with an intrinsic rotation frequency, and with local alignment interactions between circle swimmers (which are typically non-spherical).
In the monofrequent case of identical circle swimmers, one might expect that circular swimming has little impact on the physics of the Vicsek model as the absence of inertia seems to guarantee invariance of the system by global rotation of the reference frame – as for an overdamped ideal gas in a rotating bucket, where global rotations do not change the particle dynamics inside. This viewpoint receives further support by the fact that the flocking transition of Vicsek models proves invariant under rotations, as we will show. Strikingly, however, as a distinct active matter effect, this flocking transition induces long-range polar order in 2D, which spontaneously breaks rotational invariance. The consequence is that a seemingly minor modification of the Vicsek model (uniform rotations) can dramatically change its physical behaviour: while rotations do not compete with alignment interactions below the flocking transition, above it, the competition becomes nontrivial and rotations induce a new phase consisting of rotating microflocks. These microflocks emerge at a characteristic length scale which can be qualitatively predicted at mean-field level and con-

*Benno.Liebchen@.ed.ac.uk
†levis@ub.edu

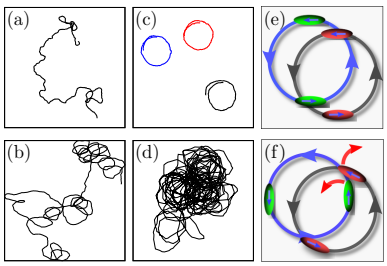

FIG. 1: Trajectory of an isolated linear (a, $\Omega = 0$) and circle swimmer (b, $\Omega = 3$). Trajectories of circle swimmers in the phase separated (c, $g\rho_0 = 2.8$, $\Omega = 0.2$) and the microflock phase (d, $g\rho_0 = 2.8$, $\Omega = 3$). (e) and (f) are cartoons illustrating the mechanism behind the formation of a macroscopic rotating droplet and a microflock pattern: for slow rotations circle swimmers phase-lock and follow circular orbits allowing for aligned configurations and the formation of large rotating clusters (e), while fast rotations leave no time to phase lock, which frustrates the alignment interactions (f).

trolled via the swim speed and the rotational frequency. This allows to use rotations as a tool to design microflock patterns. Besides fast rotations, also slow ones induce new collective effects: they allow for large-scale aggregates of phase-locked circle swimmers featuring an enhanced polarization as compared to flocks in the Vicsek model. At late times, their sizes scale linearly with system size, indicating phase separation. Following their sizes and shapes, we call these aggregates *macrodroplets*. Thus, contrasting the obvious viewpoint that identical circle swimmers do not change the collective behaviour of linear swimmers significantly, the present work shows that they lead to a rich new route to pattern formation. This route should be readily observable in identical synthetic circle swimmers (L-shaped or actuated colloids) or in magnetotactic bacteria in rotating external magnetic fields, and could be useful, for example, to design localized micro-flocks whose characteristic size can be (dynamically) controlled in the laboratory (e.g. by changing the self-propulsion velocity or the frequency of the applied field).

Besides this, our results may find further applications for understanding pattern formation in 2D suspensions of sperm cells [21] and driven protein filaments [28, 30] qualitatively matching the microflocks we observe. Note that our results may qualitatively apply even to nonidentical but synchronized biological swimmer ensembles [29].

The Chiral Active Particle model To specify our results we now define the CAP as a rotating extension of smooth variants of the Vicsek model in continuous time [10, 14, 15]: it consists of N point-like self-propelled particles with positions $\mathbf{r}_i$ and orientations $\mathbf{p}_i(t) = (\cos\theta_i, \sin\theta_i)$ which interact via an aligning pair-potential and change their direction in response to a systematic rotational force, according to:

$$\dot{\mathbf{r}}_i = v\mathbf{p}_i\,, \dot{\theta}_i = \omega + \frac{K}{\pi R_\theta^2}\sum_{j\in\partial_i}\sin(\theta_j - \theta_i) + \sqrt{2D_r}\eta_i\,, \quad (1)$$

Here, the sum runs over neighbors within a radius R_θ around particle i and $\eta_i(t)$ is a unit-variance Gaussian white noise with zero mean. In the non-interacting limit ($K = 0$), each particle performs an overdamped circular Brownian motion as shown in Fig. 1 and statistically characterised in [31]. To reduce the parameter space to its essential dimensions, we choose space and time units as R_θ and $1/D_r$. The CAP has four control parameters: the particle density $\rho_0 = NR_\theta^2/L^2$, a Peclet number $\mathrm{Pe}_r = v/(D_r R_\theta)$ measuring the persistence length in units of the alignment interaction range, $g = K/(\pi R_\theta^2 D_r)$ and $\Omega = \omega/D_r$, comparing alignment and rotational frequencies with the rotational diffusion rate. Remarkably, the phase diagram depends only on $g\rho_0$ and Ω, as we discuss below, with most interesting phenomena occurring for $g_f := g\rho_0 > 2$ and for $\Omega \sim 1$ or $\Omega > 1$. Hence, a sufficiently large number of circle swimmers ($N \sim 10^3 - 10^4$), sedimented on a quadratic surface of linear size $L \sim 10^2 - 10^3\mu$m above the standard flocking transition of the Vicsek model [38] should allow to explore our phase diagram: Rotating *E.coli* ($\omega \sim 0.1 - 1/s$ [18]; $D_r \sim 0.2/s - 1/s$) lead to $\Omega \sim 1$, whereas L-shaped swimmers ($\omega \sim 0.1 - 0.3/s$; $D_r \sim 6.10^{-4}$ [24]) allow to explore the regime $\Omega \sim 10^2 \gg 1$ and magnetotactic bacteria in rotating fields should allow to tune Ω on demand.

Pattern formation We now simulate the collective behaviour of N identical circle swimmers in a quadratic box with periodic boundary conditions (see [35] for details). For $\Omega = 0$ we reproduce the phenomenology of the Vicsek model [12, 32–34]: a disordered homogeneous phase occurs below the flocking threshold ($g < g_f$), whereas $g \gtrsim g_f$ induces a global polarization with high density bands coexisting with a disordered gas (Fig. 2 (a)). These bands eventually become unstable at higher coupling strengths, leading to homogeneous flocking. Now choosing $g > g_f$ and switching on slow rotations ($\Omega = 0.2$), we observe phase separation into a large polarly ordered dense phase and a low-density gas of incoherently rotating swimmers. Here, the presence of rotations changes the geometry of the high density region which now takes the form of a spherical cluster (macrodrop), resembling the usual liquid-gas demixing. This droplet rotates coherently but slower than individual swimmers with a frequency $\Omega^* < \Omega$ (see Fig. 1 (c), 2 (b) and Movie 1 in the Supplementary Material (SM) [35]) and grows, at late times, linearly with the system size [35]. Tuning the frequency to values $\Omega \gtrsim 1$ leads, strikingly, to a pattern of dense spots emerging with a characteristic size which is independent of the system size (see Fig. 2 (c)-(h) and Movie 3). Within each spot, particles are synchronized and form rotating microflocks: hence we call the emerging phase *the rotating microflock pattern*. This pattern resembles vortex arrays observed in sperm cells and protein filaments [21, 30].

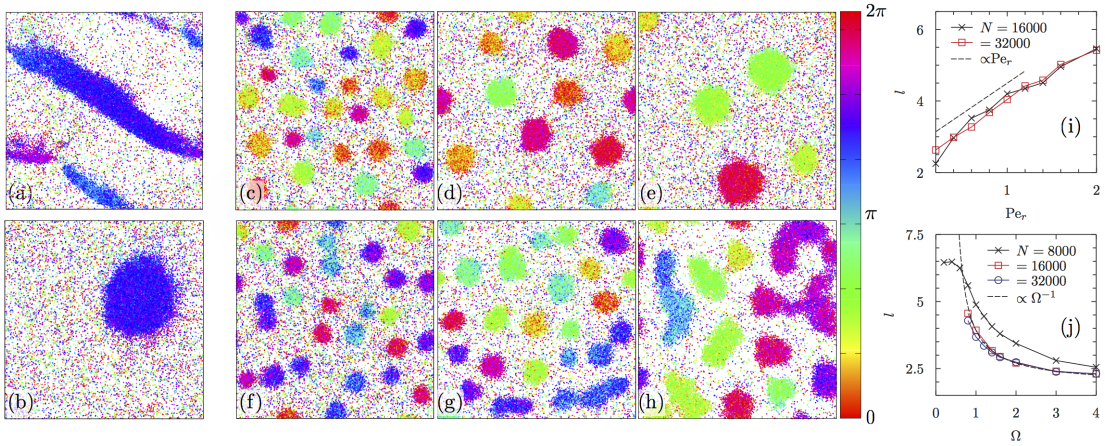

FIG. 2: Simulation snapshots for $N = 32000$ particles; colors encode particle orientations. (a, $\Omega = 0$): Traveling bands; (b, $\Omega = 0.2 < 1$): rotating macro-droplet (phase-separation) (c-h): Microflock pattern at $g\rho_0 = 2.8, \Omega = 3$ and $\mathrm{Pe}_r = 0.2$ (c), $\mathrm{Pe}_r = 1.0$ (d) and $\mathrm{Pe}_r = 2$ (e) and at $\mathrm{Pe}_r = 0.2, \Omega = 3$ and $g\rho_0 = 2.4$ (f), 3.6 (g) and 6 (h). (i, j): Microflock length scale l for $g\rho_0 = 2.8$; for $\Omega = 3$ as a function of Pe_r (i) and for $\mathrm{Pe}_r = 0.2$ as a function of Ω (j) for the system sizes shown in the key.

Hydrodynamic equations and enhanced flocking To understand the emergence of patterns and their length scales, we derive a continuum theory for the CAP in the SM [35]. Following the approaches in [36, 37] we find [35] a closed set of equations for the particle density $\rho(\mathbf{x}, t)$ and polarization density $\mathbf{w}(\mathbf{x}, t) = (w_x, w_y) = \rho\mathbf{P}$ (with $\mathbf{P}(\mathbf{x}, t)$ being the polarization field) where $|\mathbf{w}|$ measures the local degree of alignment and $\mathbf{w}/|\mathbf{w}|$ the average swimming direction.

$$\dot{\rho} = -\mathrm{Pe}_\mathrm{r}\nabla\cdot\mathbf{w} \tag{2}$$

$$\begin{aligned}\dot{\mathbf{w}} &= (g\rho - 2)\frac{\mathbf{w}}{2} - \frac{\mathrm{Pe}_\mathrm{r}}{2}\nabla\rho + \frac{\mathrm{Pe}_\mathrm{r}^2}{2b}\nabla^2\mathbf{w} - \frac{g^2}{b}|\mathbf{w}|^2\mathbf{w} \\ &+ \frac{g\mathrm{Pe}_\mathrm{r}}{4b}\left[5\nabla\mathbf{w}^2 - 10\mathbf{w}(\nabla\cdot\mathbf{w}) - 6(\mathbf{w}\cdot\nabla)\mathbf{w}\right] \\ &+ \Omega\mathbf{w}_\perp + \frac{\mathrm{Pe}_\mathrm{r}^2\Omega}{4b}\nabla^2\mathbf{w}_\perp - \frac{g^2\Omega}{2b}|\mathbf{w}|^2\mathbf{w}_\perp \\ &- \frac{g\mathrm{Pe}_\mathrm{r}\Omega}{8b}\left[3\nabla_\perp\mathbf{w}^2 - 6\mathbf{w}(\nabla_\perp\cdot\mathbf{w}) - 10(\mathbf{w}\cdot\nabla_\perp)\mathbf{w}\right]\end{aligned} \tag{3}$$

Here $b = 2(4 + \Omega^2)$, $\mathbf{w}_\perp^{(1)} = (-w_y^{(1)}, w_x^{(1)})$ and $\nabla_\perp = (-\partial_y, \partial_x)$. We first note that the disordered uniform phase (D) $(\rho, \mathbf{w}) = (\rho_0, \mathbf{0})$ solves (3) with ρ_0 being the particle density. Linearizing (3) around D (SM [35]) unveils an instability (flocking transition) $g\rho_0 > 2$, which is the same as for linear swimmers ($\Omega = 0$) showing that the emergence of long-range order is invariant to rotations. Our simulations confirm this invariance (Fig. 3)[39]. Following the flocking instability, the CAP approaches a rotating uniform phase (F), $(\rho, |\mathbf{w}|, \mathbf{w}/|\mathbf{w}|) = (\rho_0, w_0, \cos(\Omega_0 t), \sin(\Omega_0 t))$, featuring long-range order:

$$w_0 = \frac{1}{g}\sqrt{(g\rho_0 - 2)(4 + \Omega^2)} \tag{4}$$

In this phase, a macroscopic fraction of circle swimmers phase-synchronizes and rotates coherently with a frequency $\Omega_0 = \Omega\left(\frac{3}{2} - \frac{g\rho_0}{4}\right)$. This frequency reduces to the single particle frequency at the onset of flocking, but slows down as $g\rho_0$ increases. Remarkably, (4) suggests that the polarization increases with Ω, a phenomenon which we call *enhanced flocking* and confirm numerically in Fig. 3 for locally uniform macrodroplets and in [35] alongside with the predicted slowdown of rotations for (F). Physically, enhanced flocking might be based on a decrease of the average time needed for a diffusive rotating particle (which is not yet part of the flock) to align its direction with the flock. That is, rotations allow the flock to collect particles with random orientations faster.

Microflock-instability To understand the transition from (F) (which is stable only at very large $g\rho_0$ [35]) to the patterns observed above, we now perform a linear stability analysis of (F). Here, the presence of long-range order in the base state *allows* terms of order $\Omega\mathbf{w}\nabla_\perp\mathbf{w}$ to crucially impact its stability as we will see. First considering the case $\Omega = 0$ we find an oscillatory long wavelength instability along the polarization direction for $2 < g\rho_0 < 22/7$ (and a stationary long wavelength instability perpendicular to the flocking direction for $2 < g\rho_0 < 82/21$). The oscillatory instability evokes moving density fluctuations only in polarization direction and is often associated with the emergence of travelling bands in the Vicsek model [34, 37]. In the CAP we also find oscillatory long wavelength instabilities, here producing moving density fluctuations both longitudinal and perpendicular to the flocking direction which might be responsible for the emergence of (coarsening) macrodrops (Fig. 2 (b)).

Most strikingly, for larger Ω our linear stability analysis ([35]) unveils a rotation-induced oscillatory short wavelength instability which generates pattern formation

in the CAP and explains the observation of microflocks with a characteristic size (Fig. (2)); hence we call it the microflock-instability. Close to $g\rho_0 = 2$ the size of emerging microflocks scales as (see [35])

$$l \approx \frac{\pi \mathrm{Pe}_r}{2\Omega^2} \frac{|4(2-g\rho_0)+\Omega^2(12-g\rho_0)|}{\sqrt{(g\rho_0-2)(4+\Omega^2)}} \qquad (5)$$

Thus, microflocks grow linearly with Pe_r and typically decrease with Ω. If $\Omega \gg 1$, (5) yields $l \propto v/\omega$ predicting microflock sizes proportional to the (average) radius of a single circle swimmer. Our simulations confirm these scalings (Fig. 2 (i-j)): Specifically, defining the length scale l of a numerically observed structure as the value where the pair correlation function $G(l) = 1$ leads to Fig. 2: panel (i) confirms the $l \propto \mathrm{Pe}_r$ prediction and (j) shows a decrease of l with increasing Ω, revealing that the microflock size can be tuned by the microscopic parameters in our model [40]. In line with (5), we find that the microflock sizes only depend on $g\rho_0$, whereas the size of macrodroplets depends on g and ρ_0 individually [35]. Also in contrast to macrodroplets which quickly saturate to sizes of the order of the system size, microflocks coarsen slowly and may, or not, result in a phase separated state at timescales beyond experimentally relevant regimes [35].

What is the physical mechanism leading to the rotating droplet phase and the microflock pattern? While circle swimmers are effectively independent of each other at large distances in phase (D), for $g\rho_0 > 2$ they have to satisfy the rotations while being aligned on average. If interactions dominate ($g\rho_0/\Omega \gg 1$) circle swimmers can phase lock before they rotate much and follow almost ideal circles (Fig. 1 (c)). Here, they are parallel to each other all along their circular orbits (Fig. 1 (e)) and form a macroscopic rotating droplet (Fig. 2(b)). In this state, interactions support circular motion: phase locking leads to an essentially stiffly rotating many-particle object that experiences an 'average' noise, inducing only weak deviations from circular motion (Fig. 1 (c)). Conversely, when rotations dominate ($g\rho_0/\Omega < 1$), the phase locking timescale becomes comparable to the rotational timescale. This results in phase shifts among adjacent circle swimmers that frustrate, for swimmers on circular orbits, the alignment interaction (Fig. 1 (f)). The frustration, in turn, destroys circular orbits and makes large droplets of phase-locked swimmers impossible. As a result, the droplet phase breaks down opening a route to pattern formation: the resulting microflock phase can be seen as an attempt of the CAP to satisfy alignment interactions in presence of rotations but in absence of phase-locking, at least on average (see Fig. 1 (d) for a typical trajectory): rotating around a common center allows particles to avoid close-to-orthogonal configurations as the one shown in Fig. 1 (f) even in the presence of small phase shifts.

To get an overview of the parameter regimes leading to droplet and microflock patterns we summarize our results from linear stability analysis and simulations in an instability or phase diagram, Fig. 4. Although the CAP depends on four dimensionless parameters, we show in the SM [35] that the linear stability of the uniform phase is fully characterized by $g\rho_0$ and Ω. In Fig. 4, red shaded areas lead to microflock patterns while blue ones represent the rotating macrodroplet phase. Where both regimes overlap ($\Omega \sim 1$ and $g\rho_0 \gtrsim 10/3$) short and long wavelength instabilities perpendicular to the flocking direction coexist. Generally, we also find a coexisting long wavelength instability in polarization direction, which is not shown in Fig. 4 but detailed in the SM [35]. Often, the coexisting long and short wavelength instabilities are separated by a band of stable wavenumbers (Fig. 1 in [35]), suggesting that, depending on initial conditions, (F) proceeds either towards a microflock pattern or towards a macrodroplet. This suggests hysteresis in the CAP: we confirm this in Movie 5, showing phase separation for small Ω persisting even after a quench to large Ω values, which normally lead to the microflock pattern,

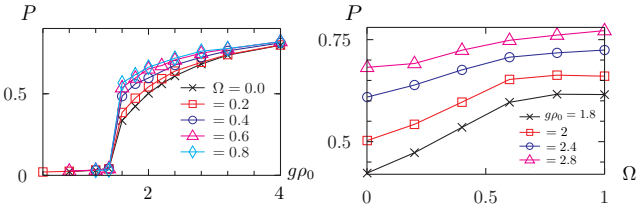

FIG. 3: Global polarization over $g\rho_0$ and Ω showing invariance of the flocking transition against rotations (left) and enhanced flocking (right) as predicted in the text.

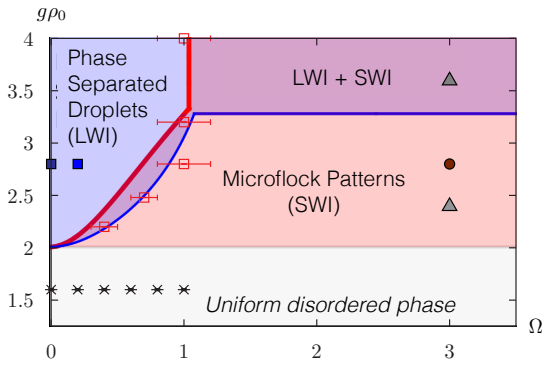

FIG. 4: Nonequilibrium phase diagram. The solid red line (obtained by linear stability analysis) and red symbols (simulations; bars represent numerical uncertainty) separate the macro-droplet phase (left blue domain) induced by a long wavelength instability (LWI) from the microflock phase (pink domain) following an oscillatory, short wavelength instability (SWI) [35]. Overlaying colours (LWI+SWI) indicate phase coexistence. The light grey domain (bottom) represents stability of the disordered uniform phase. Black symbols show the location of the flocking transition from simulations. Filled symbols show parameters of Fig. 2: (a,b) blue squares; (c-e) brown dot, (f-g) grey triangles.

when our system is initialized in phase (F).

Conclusions Chiral active matter creates long-range polar order in 2D (as polar active matter does) which violates rotational invariance and allows for nontrivial collective behaviour even in monofrequent cases: While slow rotations promote the formation of coarsening macrodroplets featuring an enhanced polarization compared to the Vicsek model, faster rotations induce microflock patterns with a characteristic size which can be tuned via the swimming speed and the rotation frequency of the underlying circle swimmers. This allows to use rotations as a design principle for microflock patterns which might be observable with autophoretic L-shaped colloids or magnetotactic bacteria.

While microflocks and macrodroplets show various distinguishing features, including the instability in the underlying mean-field equations leading to their emergence (short- vs long-wavelength instability), the Ω- and ρ_0-dependence of their sizes (Fig. 2 (j); [35]), the shape of the contained trajectories (Fig. 1) and the temporal growth-law of the largest structure ([35]), the present work does not definitely commit on whether or not the microflock pattern slowly phase-separates but invites further studies to fully characterize the nature of the transition between macrodroplets and microflocks.

Acknowledgements BL and DL gratefully acknowledge funding from a Marie Curie Intra European Fellowship (G.A. no 654908 and G.A. no 657517) within Horizon 2020.
BL and DL contributed equally to this work.

[1] J. Tailleur and M. Cates, Phys. Rev. Lett. **100**, 218103 (2008).
[2] M. E. Cates and J. Tailleur, Annu. Rev. Condens. Matter Phys. **6**, 219 (2015).
[3] I. Theurkauff, C. Cottin-Bizonne, J. Palacci, C. Ybert, and L. Bocquet, Phys. Rev. Lett. **108**, 268303 (2012).
[4] J. Palacci, S. Sacanna, A. P. Steinberg, D. J. Pine, and P. M. Chaikin, Science **339**, 936 (2013).
[5] I. Buttinoni, J. Bialké, F. Kümmel, H. Löwen, C. Bechinger, and T. Speck, Phys. Rev. Lett. **110**, 238301 (2013).
[6] D. Levis and L. Berthier, Phys. Rev. E **89**, 062301 (2014).
[7] B. Liebchen, D. Marenduzzo, I. Pagonabarraga, and M. E. Cates, Phys. Rev. Lett. **115**, 258301 (2015).
[8] T. Vicsek, A. Czirók, E. Ben-Jacob, I. Cohen, and O. Shochet, Phys. Rev. Lett. **75**, 1226 (1995).
[9] J. Toner and Y. Tu, Phys. Rev. Lett. **75**, 4326 (1995).
[10] F. Farrell, M. Marchetti, D. Marenduzzo, and J. Tailleur, Phys. Rev. Lett. **108**, 248101 (2012).
[11] J.-B. Caussin, A. Solon, A. Peshkov, H. Chaté, T. Dauxois, J. Tailleur, V. Vitelli, and D. Bartolo, Phys. Rev. Lett. **112**, 148102 (2014).
[12] A. P. Solon, H. Chaté, and J. Tailleur, Phys. Rev. Lett. **114**, 068101 (2015).
[13] Kaiser, A and Löwen, H, *Phys. Rev. E* **87**, 032712 (2013).
[14] Peruani, F. and Deutsch, A. and Bär, M., Eur. Phys. J. **157**, 111 (2008).
[15] Chepizhko, O. and Peruani, F., *Phys. Rev. Lett.* **111**, 160604 (2013).
[16] H. C. Berg and L. Turner, Biophys. J. **58**, 919 (1990).
[17] W. R. DiLuzio, L. Turner, M. Mayer, P. Garstecki, D. B. Weibel, H. C. Berg, and G. M. Whitesides, Nature **435**, 1271 (2005).
[18] E. Lauga, W. R. DiLuzio, G. M. Whitesides, and H. A. Stone, Biophys. J **90**, 400 (2006).
[19] R. Di Leonardo, D. DellArciprete, L. Angelani, and V. Iebba, Phys. Rev. Lett. **106**, 038101 (2011).
[20] B. M. Friedrich and F. Jülicher, Proc. Natl. Acad. Sci. **104**, 13256 (2007).
[21] I. H. Riedel, K. Kruse, and J. Howard, Science **309**, 300 (2005).
[22] K. Ērglis, Q. Wen, V. Ose, A. Zeltins, A. Sharipo, P. A. Janmey, and A. Cēbers, Biophys. J. **93**, 1402 (2007).
[23] A. Cēbers, J. Magn. Magn. Mater. **323**, 279 (2011).
[24] F. Kümmel, B. ten Hagen, R. Wittkowski, I. Buttinoni, R. Eichhorn, G. Volpe, H. Löwen, and C. Bechinger, Phys. Rev. Lett. **110**, 198302 (2013).
[25] B. ten Hagen, F. Kümmel, R. Wittkowski, D. Takagi, H. Löwen, and C. Bechinger, Nat. Commun. **5**, 4829 (2014).
[26] H. Löwen, Eur. Phys. J. Special Topics **225**, 2319 (2016).
[27] B. Friedrich, Eur. Phys. J. Special Topics **225**, 2353 (2016).
[28] J. Denk, L. Huber, E. Reithmann, and E. Frey, Phys. Rev. Lett. **116**, 178301 (2016).
[29] B. Liebchen, M. E. Cates, and D. Marenduzzo, Soft Matter **12**, 7259 (2016).
[30] M. Loose and T. J. Mitchison, Nat. Cell Biol. **16**, 38 (2014).
[31] S. van Teeffelen and H. Löwen, Phys. Rev. E **78**, 020101 (2008).
[32] T. Vicsek and A. Zafeiris, Phys. Rep. **517**, 71 (2012).
[33] G. Grégoire and H. Chaté, Phys. Rev. Lett. **92**, 025702 (2004).
[34] S. Mishra, A. Baskaran, and M. C. Marchetti, Phys. Rev. E **81**, 061916 (2010).
[35] See Supplementary Material at doi:... (????).
[36] D. S. Dean, J. Phys. A **29**, L613 (1996).
[37] E. Bertin, M. Droz, and G. Grégoire, J. Phys. A **42**, 445001 (2009).
[38] Following Onsager theory, for particles with a large aspect ratio ($\gtrsim 10$) steric repulsion should be sufficient to generate (local) alignment at moderate area fractions ($\gtrsim 0.2$).
[39] We find a flocking transition close to but slightly below the theoretical prediction, as previously noted in [10].
[40] In Fig. 2 (j) we only show l within the regime where microflocks are approximately isotropic. For larger g, the length scale l as defined by the pair correlation function depends on the microflock shape and doesn't represent their length scale in a unique way.

View publication stats